Available online at www.sciencedirect.com
ScienceDirect
Journal of the European Ceramic Society 29 (2009) 139–144
www.elsevier.com/locate/jeurceramsoc

Mechanochemical synthesis of nanoparticulate ZnO–$ZnWO_4$ powders and their photocatalytic activity

Aaron Dodd [a,c,*], Allan McKinley [a], Takuya Tsuzuki [b], Martin Saunders [c]

[a] School of Biomedical, Biomolecular and Chemical Sciences, The University of Western Australia, 35 Stirling Highway, Crawley, WA 6009, Australia
[b] Advanced Nanotechnology Limited, 112 Radium Street, Welshpool, WA 6106, Australia
[c] Centre for Microscopy, Characterisation and Analysis, The University of Western Australia, 35 Stirling Highway, Crawley, WA 6009, Australia

Received 26 March 2008; received in revised form 28 May 2008; accepted 30 May 2008
Available online 9 July 2008

Abstract

In this study, mechanochemical reaction systems with H_2WO_4 as a precursor were investigated for the synthesis of nanoparticulate powders of WO_3, $ZnWO_4$, and dual-phase $(ZnWO_4)_x(ZnO)_{1-x}$. The objective was to establish whether mechanochemical processing can be used to manufacture high activity photocatalysts in the ZnO–WO_3 system. Milling and heat treatment of H_2WO_4 + 12NaCl was found to result in the formation of irregularly shaped platelets of a sodium tungstate rather than nanoparticles of WO_3. Powders of single-phase $ZnWO_4$ and dual-phase $(ZnWO_4)_x(ZnO)_{1-x}$ were successfully synthesised by incorporating H_2WO_4 into the $ZnCl_2 + Na_2CO_3$ + 4NaCl reactant mixture. The photocatalytic activity of these powders was evaluated using the spin-trapping technique with electron paramagnetic resonance spectroscopy. It was found that the photocatalytic activity decreased with the $ZnWO_4$ content. This decrease in activity was attributed to the larger average particle size of the $ZnWO_4$ component compared to the ZnO, which reduced the surface area available for interfacial transfer of the photogenerated charge carriers.

Keywords: A. Milling; A. Powders-solid state reaction; B. Platelets; C. Chemical properties; D. ZnO

1. Introduction

The absorption of sufficiently energetic UV-light by a wide band-gap semiconductor results in the creation of electrons and holes through a process of electronic excitation between the valence and conductions bands. Once created, these photogenerated charge carriers are able to migrate to the surface of the semiconductor and undergo redox reactions with adsorbed molecules. This process, known as heterogeneous photocatalysis, is currently of significant research interest as a method for the destruction of intractable chemical waste.[1]

Mechanochemical processing has recently attracted attention as a means of manufacturing nanoparticulate photocatalysts as it allows significant control to be exerted over the agglomeration and particle size.[2–5] It is known from previous experimental studies that there exists an optimal particle size for which the activity of a particulate photocatalyst is maximized.[2,6] As a consequence, an ability to control agglomeration and particle size provides a means of tailoring the photocatalytic activity for specific technological applications.

In addition to offering control of microstructural properties, the mechanochemical synthesis technique is also capable of manufacturing coupled photocatalysts, which exhibit heightened activity. In an earlier study, it was shown that $(SnO_2)_x(ZnO)_{1-x}$ can successfully be synthesised by mechanochemical reaction of $SnCl_2$ and $ZnCl_2$ with Na_2CO_3. This dual oxide powder of $(SnO_2)_{0.1}(ZnO)_{0.9}$ was found to be significantly more active than either SnO_2 or ZnO powders that were synthesised using similar processing conditions.[3]

Previous experimental studies have shown that wet chemical techniques can successfully manufacture nanoparticulate photocatalysts in the ZnO–WO_3 system, including single-phase $ZnWO_4$[7–10] and dual-phase $(ZnO)_x(WO_3)_{1-x}$.[11] It is thus of interest to establish whether mechanochemical processing can likewise be used to synthesise high activity photocatalysts in the ZnO–WO_3 system but with enhanced control over particle size

* Corresponding author at: Mail Stop M313, School of Biomedical, Biomolecular and Chemical Sciences, The University of Western Australia, 35 Stirling Highway, Crawley, WA 6009, Australia. Tel.: +61 8 6488 4485; fax: +61 8 6488 4485.
E-mail address: acd@cyllene.uwa.edu.au (A. Dodd).

0955-2219/$ – see front matter © 2008 Elsevier Ltd. All rights reserved.
doi:10.1016/j.jeurceramsoc.2008.05.027

and microstructural properties. To this end, mechanochemical reaction systems with H_2WO_4 as a precursor were investigated for the synthesis of nanoparticulate WO_3, $ZnWO_4$, and dual-phase $(ZnWO_4)_x(ZnO)_{1-x}$ powders. The photocatalytic activity of these powders was characterised by measuring the concentration of photogenerated hydroxyl radicals using the spin-trapping technique with electron paramagnetic resonance spectroscopy.

2. Experimental techniques

2.1. Powder synthesis

Aqueous powder slurries were manufactured by a three stage process consisting of mechanical milling, low-temperature heat treatment, and washing. In the first stage of processing, reactant mixtures were milled for 6 h within a hardened steel vial using a Spex 8000 mixer/mill. All millings used a 10 g-powder charge with twenty 9.5-mm stainless steel balls as the grinding media. To ensure an inert atmosphere during milling, the grinding media and reactants were loaded into the vial whilst within a high-purity argon-filled glovebox.

Following milling, the reactant mixtures were heat-treated in air for 1 h at 500 °C. In the final stage of processing, the NaCl reaction by-product was removed by repeated washing with deionised water. Washed slurries were divided into two portions. The first portion of slurry was dried so as to allow analysis of the powder by X-ray diffraction and BET gas adsorption. The second portion was used in the undried state to prepare samples for transmission electron microscopy and photocatalytic testing.

2.2. Characterisation techniques

The chemical evolution of the reactant mixtures during processing was monitored by X-ray diffraction (XRD) using a Siemens D5000 diffractometer with Cu K_α radiation. The average crystallite size of the ZnO powders was estimated from the full-width half-maximum of the diffraction peaks using the Scherrer equation.[12]

The specific surface area of the washed powders was measured by five-point BET gas adsorption using a Micromeritics Tristar instrument. All powders were vacuum degassed at 150 °C for 1 h prior to analysis. For the single-phase powders, the specific surface area was used to derive estimates of the average particle diameter by assuming that the powder consisted of dispersed spherical particles with no porosity. The average particle diameter could therefore be related to the specific surface area through $D = 6/S\rho$, where D is the average particle diameter, S is the specific surface area, and ρ is the density.

Washed powders were examined by transmission electron microscopy (TEM) using a JEOL 2000FX microscope with a beam energy of 80 keV. High-resolution TEM images were taken using a JEOL 3000F microscope with a beam energy of 300 keV. Samples for TEM were prepared by ultrasonically dispersing a small quantity of the aqueous slurry in a 0.10 wt.% solution of stearic acid in hexane and then evaporating a drop of this dispersion on a carbon coated specimen grid.

2.3. Photocatalytic testing

Samples for photocatalytic testing were prepared by diluting the washed slurries down to a solids content of 0.02 wt.% with Milli-Q water. The diluted slurries were subjected to intense ultrasonication for 15 min in order to disperse the particles within the suspension. Immediately prior to measurement of the photocatalytic activity, 1 mL of a 30 mM solution of 5,5-dimethyl-1-pyrroline N-oxide (DMPO) spin-trap was added to 10 mL of the powder suspension.

The photocatalytic activity of the powder suspensions was evaluated by measuring the hydroxyl radical concentration using the spin-trapping technique with electron paramagnetic resonance (EPR) spectroscopy.[13–15] Samples were irradiated with 300 nm light from a 1 kW Hg–Xe lamp whilst within a quartz flat cell that was located in the cavity of the EPR spectrometer. A monochromator was attached to the lamp to select the irradiation wavelength. The concentration of photogenerated hydroxyl radicals was measured after 50 s of irradiation by recording the intensity of the first central line of the first derivative EPR spectrum corresponding to the DMPO-OH spin adduct.

3. Results and discussion

3.1. Mechanical grinding of H_2WO_4 with NaCl

Previous experimental studies have shown that oxide nanoparticles can be synthesised through a process based on mechanical grinding of a suitable precursor with an inert salt diluent.[16–18] In this process, mechanical grinding disintegrates and disperses the precursor into the salt matrix. Heat treatment of the as-milled powder is then used to decompose the precursor into the desired oxide phase, which is subsequently recovered from the salt matrix by washing with a suitable solvent. This technique has successfully been used to synthesise nanoparticulate powders of a variety of oxide materials, including Fe_2O_3,[16] $CoFe_2O_3$,[17] and Y_2O_3.[18]

In this study, we attempted to manufacture nanoparticulate WO_3 by a similar process using H_2WO_4 as the precursor and NaCl as the salt diluent. It was expected that mechanical milling of $H_2WO_4 + 12NaCl$ would result in the formation of a nanocrystalline powder consisting of H_2WO_4 grains dispersed within the NaCl matrix. Low-temperature calcination could then be used to form nanoparticles of WO_3 through

$$H_2WO_4 + 12NaCl \rightarrow WO_3 + 12NaCl + H_2O_{(g)} \quad (1)$$

However, it was found that the NaCl diluent phase was not inert during processing. This is illustrated in Fig. 1, which shows the XRD pattern of $H_2WO_4 + 12NaCl$ following (a) mixing in a mortar and pestle, (b) milling for 4 h, (c) heat treatment at 500 °C for 1 h, and (d) washing. It can be seen that milling and heat treatment of the reactant mixture resulted in the formation of a composite powder consisting of an unknown phase and NaCl. This unknown phase was found to be insoluble and was successfully recovered by washing with deionised water.

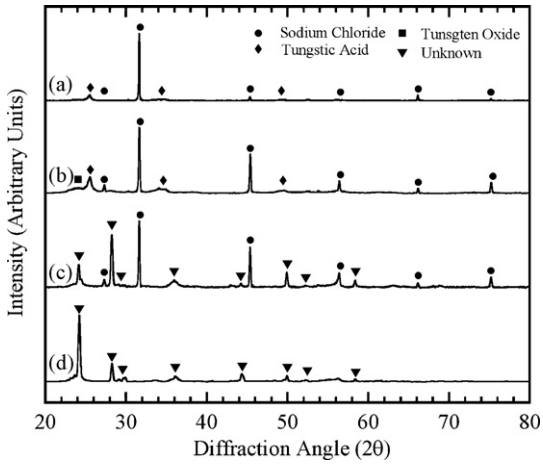

Fig. 1. XRD pattern of H_2WO_4 + 12NaCl following (a) mixing in a mortar and pestle, (b) milling for 6 h, (c) heat treatment at 500 °C for 1 h, and (d) washing.

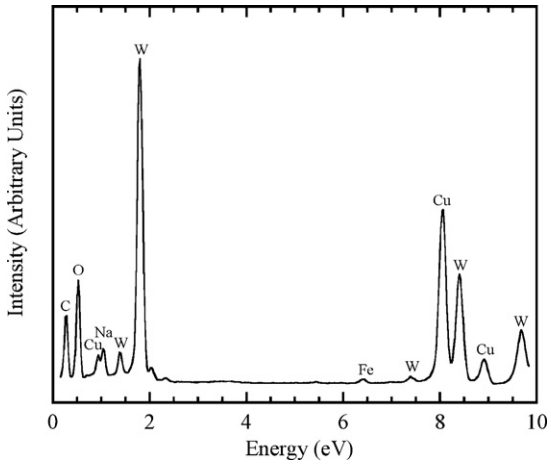

Fig. 2. EDS spectra of the washed powder synthesised from H_2WO_4 + 12NaCl.

The XRD pattern of the washed powder could not be definitively matched to any pattern in the JCPDS database. However, the major diffraction peaks appear to correspond with those of $Na_2W_3O_{19}$ (JCPDS #28-1157), which suggests that the powder may be a sodium tungstate with a related crystal structure. X-ray microanalysis provides confirmation that the powder is a sodium tungstate. As shown in Fig. 2, the energy-dispersive X-ray spectrum of the washed powder consists of peaks corresponding to sodium, tungsten, and oxygen. The carbon and copper peaks are attributable to the carbon coated copper sample grid. The iron peak is either instrumental or an impurity in the powder that was acquired from the grinding media.

Previous experimental studies have shown that H_2WO_4 and WO_3 are unstable in the presence of molten NaCl.[19,20] For example, an investigation into the synthesis of metallic tungsten by Kahlenberg and Kahlenberg[19] found that the addition of H_2WO_4 to molten NaCl results in the formation of sodium

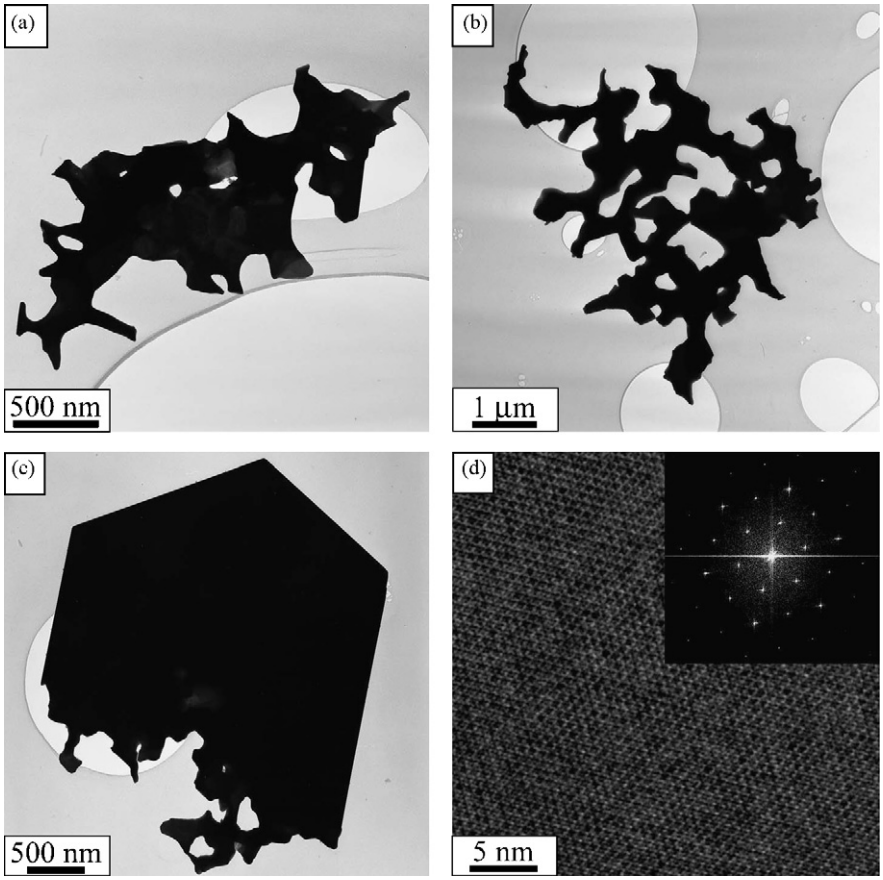

Fig. 3. Low- and high-resolution TEM images of the washed powder synthesised from H_2WO_4 + 12NaCl. The inset in (d) is the Fourier transform of the lattice image.

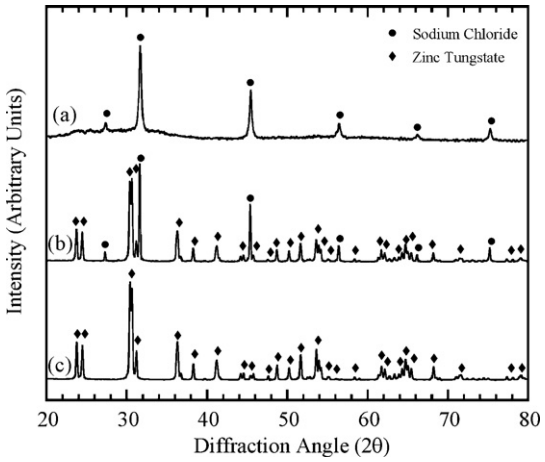

Fig. 4. XRD pattern of $H_2WO_4 + ZnCl_2 + Na_2CO_3 + 4NaCl$ following (a) milling for 6 h, (b) heat treatment at 500 °C for 1 h, and (c) washing.

tungstates through the evolution of $HCl_{(g)}$. In the present work, it is notable that chemical reaction of the H_2WO_4 precursor to form a sodium tungstate occurred well below the melting point of NaCl (~801 °C). This suggests that the microstructural refinement and accumulation of lattice defects arising from the mechanical milling enhanced the chemical reactivity such that melting was not necessary for reaction.

Fig. 3 shows TEM images of the washed powder that was synthesised from $H_2WO_4 + 12NaCl$. As shown in (a) and (b), the powder predominantly consists of irregularly shaped plate-like particles. However, as illustrated by (c), there are also a few particles with clear facets that reflect the underlying hexagonal crystal symmetry of the compound, which is illustrated by HRTEM and the corresponding Fourier transform in Fig. 3(d).

3.2. Synthesis of ZnO and $ZnWO_4$

The synthesis of nanoparticulate ZnO by mechanochemical reaction of $ZnCl_2$ with Na_2CO_3 has previously been reported.[2,5] In these earlier studies, it was found that chemical reaction of the precursors occurred during milling with the consequent formation of nanocrystalline $ZnCO_3$ grains embedded within a matrix of NaCl. Subsequent heat treatment and washing yielded an aqueous slurry of well-dispersed ZnO nanoparticles. The same basic method was employed in the present study. A reactant mixture corresponding to $ZnCl_2 + Na_2CO_3 + 4NaCl$ gave a ZnO powder with specific surface area of 23.9 m^2/g.

The basic reaction system for the synthesis of ZnO was subsequently extended to manufacture $ZnWO_4$. This simply involved incorporating H_2WO_4 into the reactant mixture, as given by

$$H_2WO_4 + ZnCl_2 + Na_2CO_3 + 4NaCl \rightarrow ZnWO_4 + 6NaCl + H_2O_{(g)} + CO_{2(g)} \quad (2)$$

The phase evolution of this reactant mixture during processing was found to be similar to that displayed by the ZnO synthesis. This is illustrated in Fig. 4, which shows the XRD pattern of $H_2WO_4 + ZnCl_2 + Na_2CO_3 + 4NaCl$ following (a) milling for 6 h, (b) heat treatment at 500 °C for 1 h, and (c) washing. Following milling, the pattern consists of broadened diffraction peaks corresponding to nanocrystalline NaCl. Subsequent heat treatment resulted in a sharpening of the NaCl peaks and the appearance of new diffraction peaks corresponding to $ZnWO_4$. Following washing, only the $ZnWO_4$ peaks remained, which indicates the successful removal of the NaCl salt by-product. The successful synthesis of $ZnWO_4$ indicates that formation of the sodium tungstate phase is thermodynamically unfavorable in the presence of anhydrous $ZnCl_2$.

The only peaks evident in the XRD pattern of the as-milled powder are those of NaCl. The absence of any other peaks indicates that the other phases present in the as-milled powder were either amorphous or at least poorly crystalline, as has been found in previous studies of mechanochemical reaction systems.[5] This suggests that the as-milled powder was a nanocrystalline composite consisting of poorly crystalline H_2WO_4, and $ZnCO_3$ embedded in NaCl. Formation of $ZnWO_4$ occurred during heat treatment through decomposition of the H_2WO_4 and $ZnCO_3$ into oxides and their subsequent interdiffusion.

Analysis of the diffraction peak breadth of the washed $ZnWO_4$ using the Scherrer equation gave a crystallite size of approximately 40 nm. Analysis by BET gas adsorption gave a specific surface area of 8.1 m^2/g, which corresponds to an average particle diameter of approximately 94 nm. The discrepancy between the XRD crystallite size and BET particle size indicates that the powder contained some degree of hard agglomeration. Such agglomeration would decrease the exposed surface area of the powder and thereby increase the apparent particle size. The presence of hard agglomeration in the washed powder was confirmed by TEM imaging, as shown in Fig. 5. The HRTEM image shows three particles lying side by side. It can be seen that certain lattice planes are continuous across the particle boundaries, which indicates the presence of a solid bridge.

Two key factors affecting the particle size and degree of agglomeration of the final $ZnWO_4$ powder were the milling duration and the temperature of the post-milling heat treatment. The duration of milling would have determined the extent to which the H_2WO_4 precursor had been broken-up and dispersed within the powder charge. Insufficient breakage of the H_2WO_4 precursor would inevitably yield coarse and agglomerated particles of $ZnWO_4$ during the subsequent heat treatment step.[18] The temperature of the post-milling heat treatment would have affected the final particle size of the $ZnWO_4$ product by determining the extent of particle growth.[2]

3.3. Synthesis of $(ZnWO_4)_x(ZnO)_{1-x}$

The successful synthesis of single-phase $ZnWO_4$ by incorporating one molar equivalent of H_2WO_4 into the ZnO synthesis system suggests that it should be possible to synthesise dual-phase $(ZnWO_4)_x(ZnO)_{1-x}$ powders by simply varying the amount of H_2WO_4 in the reactant mixture. In order to test this possibility, a series of powders were prepared from $xH_2WO_4 + ZnCl_2 + Na_2CO_3 + 4NaCl$ reactant mixtures, where $x = 0.25$, 0.50, and 0.75. It was found that milling, heat treatment, and washing of these reactant mixtures does indeed yield dual-phase powders consisting of ZnO and $ZnWO_4$. Measure-

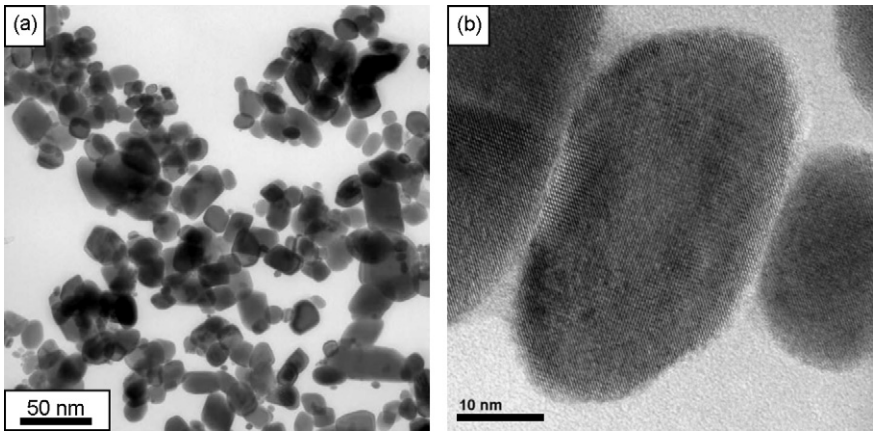

Fig. 5. Low (a) and high (b) magnification TEM images of the washed $ZnWO_4$ powder.

ment of the XRD peak breadth revealed that the crystallite size of the component phases was invariant with respect to the overall composition of the powder. The average crystallite size of the ZnO and $ZnWO_4$ phases was approximately 29 and 40 nm, respectively.

Fig. 6 shows bright field TEM images of $(ZnWO_4)_x(ZnO)_{1-x}$ powders containing (a) 0 (b) 25, (c) 50, and (d) 75 mol.% $ZnWO_4$. The single oxide powder of ZnO consists of equiaxed nanoparticles with a reasonably narrow size distribution. In contrast, the dual oxide powders are characterised by a bimodal particle size distribution. This is consistent with the XRD crystallite measurements, which indicated that the $ZnWO_4$ particles were substantially larger than the ZnO.

3.4. Photocatalytic activity of $(ZnWO_4)_x(ZnO)_{1-x}$

Fig. 7 shows the specific surface area and DMPO-OH yield of each $(ZnWO_4)_x(ZnO)_{1-x}$ powder. It can be seen that the single-phase ZnO powder was characterised by the highest specific surface area and gave the highest DMPO-OH yield, which indicates that it was the most active photocatalyst in the $(ZnWO_4)_x(ZnO)_{1-x}$ system. The specific surface area and

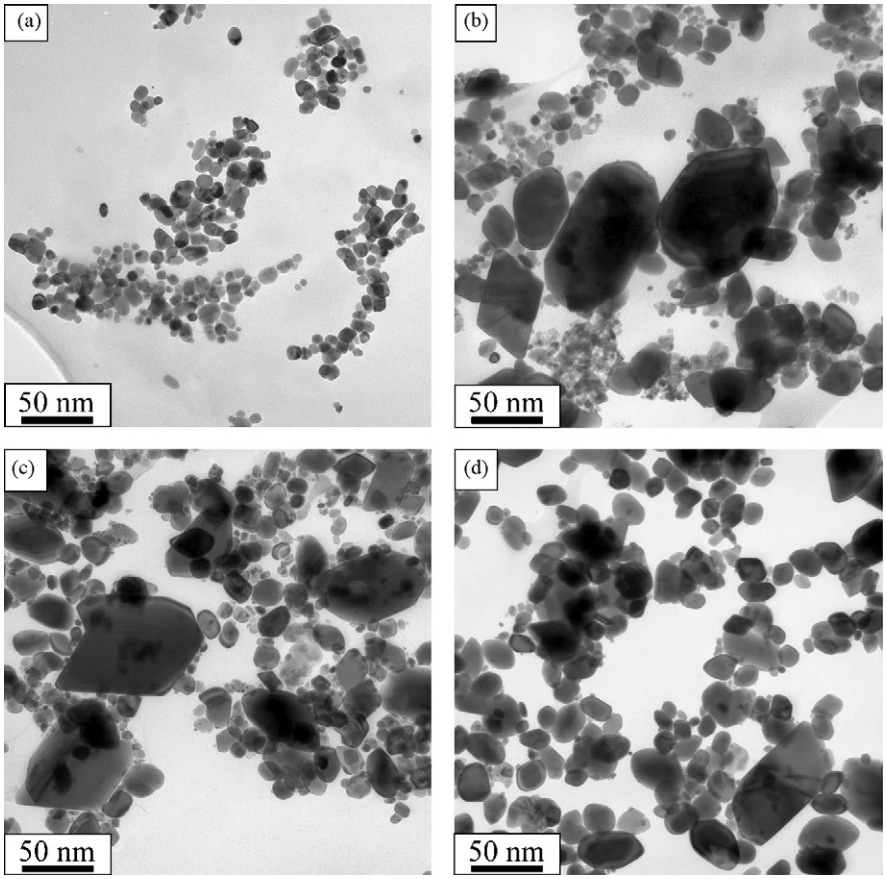

Fig. 6. Bright field TEM images of $(ZnWO_4)_x(ZnO)_{1-x}$ powders containing (a) 0, (b) 25, (c) 50, and (d) 75 mol.% $ZnWO_4$.

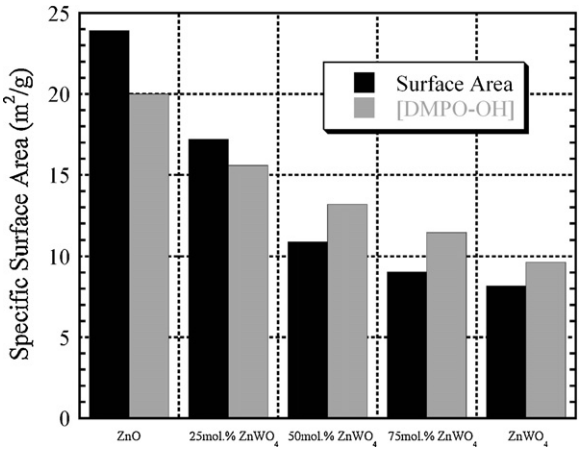

Fig. 7. Specific surface area and DMPO-OH yield as a function of $ZnWO_4$ content for aqueous suspensions of the $(ZnWO_4)_x(ZnO)_{1-x}$ powders.

DMPO-OH yield progressively declined with the $ZnWO_4$ content and reached their minimum for the single-phase $ZnWO_4$ powder.

Expressed in terms of the DMPO-OH yield per unit of specific surface area, the single-phase $ZnWO_4$ powder is characterised by a level of photocatalytic activity that is similar to that of the single-phase ZnO. This is consistent with previous experimental studies regarding the photocatalytic activity of nanoparticulate $ZnWO_4$, which have found that its intrinsic activity is comparable to other commonly utilized semiconductor photocatalysts.[7–10] For example, Fu et al.[7] found that $ZnWO_4$ that was synthesised by hydrothermal processing showed better activity for the degradation of formaldehyde than P25 TiO_2.

The progressive decline in photocatalytic activity of the $(ZnWO_4)_x(ZnO)_{1-x}$ powders with the increasing $ZnWO_4$ content indicates that there is no beneficial effect arising from the coupling of ZnO with $ZnWO_4$. It would appear that the overall photocatalytic activity of the dual-phase powders in the $(ZnWO_4)_x(ZnO)_{1-x}$ system is merely the sum of the activities of the individual component phases.

4. Summary and conclusions

The results obtained in this study demonstrate that the basic mechanochemical reaction system for the synthesis of nanoparticulate ZnO can be extended to allow the synthesis of single-phase $ZnWO_4$ and dual-phase $(ZnWO_4)_x(ZnO)_{1-x}$ powders. Analysis of the single-phase $ZnWO_4$ using the spin-trapping technique with EPR spectroscopy revealed that its intrinsic photocatalytic activity is similar to that of ZnO. Measurement of the photocatalytic activity of the dual-phase $(ZnWO_4)_x(ZnO)_{1-x}$ powders showed that there is no beneficial effect to be gained from coupling $ZnWO_4$ with ZnO.

Acknowledgements

This research was supported by the Australian Research Council under Linkage Project LP0349177 and was carried out using facilities at the Centre for Microscopy, Characterisation and Analysis, which is supported by University, State and Federal Government funding.

References

1. Hoffman, M., Martin, S., Choi, W. and Bahnemann, D., Environmental applications of semiconductor photocatalysis. *Chem. Rev.*, 1995, **95**, p69.
2. Dodd, A. C., McKinley, A. J., Saunders, M. and Tsuzuki, T., Effect of particle size on the photocatalytic activity of nanoparticulate zinc oxide. *J. Nanopart. Res.*, 2006, **8**, 43.
3. Dodd, A. C., McKinley, A. J., Saunders, M. and Tsuzuki, T., Mechanochemical synthesis of nanocrystalline SnO_2–ZnO photocatalysts. *Nanotechnology*, 2006, **17**, 692.
4. Billik, P., Plesch, G., Brezova, V., Kuchta, L., Valko, M. and Mazur, M., Anatase TiO_2 nanocrystals prepared by mechanochemical synthesis and their photochemical activity studied by EPR spectroscopy. *J. Phys. Chem. Solids*, 2007, **68**, 1112.
5. Tsuzuki, T. and McCormick, P. G., ZnO nanoparticles synthesised by mechanochemical processing. *Scripta Mater.*, 2001, **44**, 1731.
6. Zhang, Z., Wang, C.-C., Zakaria, R. and Ying, J., Role of particle size in nanocrystalline TiO_2-based photocatalysts. *J. Phys. Chem. B*, 1998, **102**, 10871.
7. Fu, H., Li, J., Zhang, L. and Zhu, Y., Photocatalytic activities of a novel $ZnWO_4$ catalyst prepared by a hydrothermal process. *Appl. Catal. A*, 2006, **306**, 58.
8. Huang, G., Zhang, C. and Zhu, Y., $ZnWO_4$ photocatalyst with high activity for degradation of organic contaminants. *J. Alloys Compd.*, 2007, **432**, 269.
9. Fu, H., Chengsi, P., Zhang, L., Zhu, Y. and Synthesis, Characterization and photocatalytic properties of nanosized Bi_2WO_4, $PbWO_4$ and $ZnWO_4$ catalysts. *Mater. Res. Bull.*, 2007, **42**, 696.
10. Huang, G. and Zhu, Y., Synthesis and photocatalytic performance of $ZnWO_4$ catalyst. *Mater. Sci. Eng. B*, 2007, **139**, 201.
11. Sakthivel, S., Geissen, S., Bahnemann, D., Murugesan, V. and Vogelpohl, A., Enhancement of photocatalytic activity by semiconductor heterojunctions: α-Fe_2O_3, WO_3 and CdS deposited on ZnO. *J. Photochem. Photobiol. A*, 2002, **148**, 283.
12. Cullity, B., *Elements of X-ray diffraction* (*2nd ed.*). Addison-Wesley, Reading, 1978.
13. Jaeger, C. D., Bard, A. J. and Spin Trapping, Electron spin resonance detection of radical intermediates in the photodecomposition of water at TiO_2 particulate systems. *J. Phys. Chem.*, 1979, **83**, 3146.
14. Janzen, E. G., Spin trapping. *Acc. Chem. Res.*, 1971, **4**, 31.
15. Grela, M. A., Coronel, M. E. J. and Colussi, A. J., Quantitative spin-trapping studies of weakly illuminated titanium dioxide sols. Implications of the mechanism of photocatalysis. *J. Phys. Chem.*, 1996, **100**, 16940.
16. Liu, X., Ding, J. and Wang, J., An α-Fe_2O_3 powder of nanosized particles via precursor dispersion. *J. Mater. Res.*, 1999, **14**, 3355.
17. Shi, Y., Ding, J. and Yin, H., $CoFe_2O_4$ nanoparticles prepared by the mechanochemical method. *J. Alloys Compd.*, 2000, **308**, 290.
18. Dodd, A. C. and McCormick, P. G., Synthesis of nanocrystalline yttrium oxide powders by mechanochemical processing. *J. Metastable Nanocryst. Mats.*, 2004, **20–21**, 319.
19. Kahlenberg, L. and Kahlenberg, H., The preparation of metallic tungsten and some of its alloys. *J. Am. Electrochem. Soc.*, 1924, **46**, 181.
20. Mobin, M., Malik, A. U. and Ahmad, High temperature interactions of metal oxides with NaCl. *J. Less Common Metals*, 1990, **160**, 1.